Article No. jmbi.1999.2593 available online at http://www.idealibrary.com on IDEAL J. Mol. Biol. (1999) 287, 163–171

JMB

Site-directed Spin-labeling Reveals the Orientation of the Amino Acid Side-chains in the E-F Loop of Bacteriorhodopsin

Matthias Pfeiffer[2], Thomas Rink[1], Klaus Gerwert[1], Dieter Oesterhelt[2] and Heinz-Jürgen Steinhoff[1]*

[1]*Lehrstuhl für Biophysik Ruhr-Universität Bochum 44780 Bochum, Germany*

[2]*Max-Planck-Institut für Biochemie, Am Klopferspitz 18 a, 82152 Martinsried, Germany*

**Corresponding author*

Due to high temperature factors and the lack of considerable electron density, electron microscopy and X-ray experiments on the cytoplasmic E-F loop of bacteriorhodopsin result in a variety of structural models. As the experimental conditions regarding ionic strength, temperature and the presence of detergents may affect the structure of the E-F loop, we employ electron paramagnetic resonance and site-directed spin-labeling to study the structure of this loop under physiological conditions. The amino acid residues at positions 154 to 171 were replaced by cysteine residues and derivatized with a sulfhydryl-specific nitroxide spin label one by one. The conventional and power saturation electron paramagnetic spectroscopy provide the mobility of the nitroxide and its accessibility to dissolved molecular oxygen and membrane-impermeable chromium oxalate in the respective site. The results show that K159 and A168 are located at the water-lipid interface of helices E and F, respectively. The orientation of the amino acid side-chains in the helical regions from positions 154 to 159 and 166 to 171 were found to agree with published structural data for bacteriorhodopsin. In the residue sequence from positions 160 to 165 the EPR data yield evidence for a turned loop structure with the side-chains of M163 and S162 oriented towards the proton channel and the water phase, respectively.

© 1999 Academic Press

Keywords: electron paramagnetic resonance; bacteriorhodopsin; saturation parameter; site-directed spin-labeling; retinal proteins

Introduction

The transmembrane protein bacteriorhodopsin uses light energy to pump protons from the cytoplasma of halobacteria into the extracellular space (for reviews, see e.g. Tittor, 1991; Lanyi, 1993; Oesterhelt, 1998). The absorption of a photon by its chromophore all-*trans* retinal causes isomerization to 13-*cis* retinal and initiates a series of proton transfer steps and conformational rearrangements in the protein. The catalytic cycle results in the net translocation of a proton across the membrane. Intermediates of the catalytic cycle distinguished by their different absorption maxima can be analyzed by flash-induced transient absorption changes, and spectroscopically discernible intermediates J, K, L, M, N and O have been described (Xie *et al.*, 1987; Varo & Lanyi, 1991; Lozier *et al.*, 1992; Hessling *et al.*, 1993). The temporal sequence of rise and decay of these intermediates defines the so called photocycle of bacteriorhodopsin initiated by photon absorption. Point mutations and biophysical studies have characterized specific configurational states of the retinal, the protonation states of both its Schiff base with the protein and of certain amino acid residues, and the conformation of the protein. After light-induced isomerization, the molecule passes through the short-lived intermediates J, K and L before it reaches the M intermediate. The L-M transition is accompanied by the transfer of a proton from the Schiff base, which connects retinal to K216, to D85 and sub-

Abbreviations used: BR, bacteriorhodopsin; DPPH, diphenylpicrylhydrazyl; DMSO, dimethylsulfoxide; EPR, electron paramagnetic resonance; MTSSL, (1-oxyl-2,2,5,5-tetramethylpyrroline-3-methyl)methanethiosulfonate; CROX, chromium oxalate.

E-mail address of the corresponding author: hjs@bph.ruhr-uni-bochum.de

0022-2836/99/110163–09 $30.00/0

© 1999 Academic Press

sequent proton transfer to the extracellular space. A change in accessibility of the Schiff base from the extracellular to the cytoplasmic half-channel during the M state divides this intermediate into two substates, M_{EC} and M_{CP} (Oesterhelt, 1998). Subsequently, reprotonation of the Schiff base by D96 occurs during N formation. D96 finally receives a proton from the cytoplasmic side and the catalytic cycle is completed after reisomerization to the all-*trans* state and rechange of accessibility to the extracellular side. Several other residues and a hydrogen bond network were found to be involved in the proton transfer process (Oesterhelt, 1998; Wickström, 1998). Conformational changes occur in the second half of the photocycle, starting with the M intermediate, and are suggested to be involved in the accessibility change of the active center and optimization of the proton transfer rates (Sass *et al*., 1997).

A challenging goal of biophysical studies on bacteriorhodopsin (BR) is the time-resolved analysis of its structure during the catalytic cycle in order to fully understand the mechanism of vectorial transport at the atomic level as a paradigm for many more transport proteins in bioenergietics. Recently, density maps from two-dimensional crystals of the BR ground state were obtained using cryo-electron microscopy (Henderson *et al*., 1990; Grigorieff *et al*., 1996; Kimura *et al*., 1997). New methods concerning the three-dimensional crystallization of membrane proteins and the availability of intense X-ray point sources provided also a X-ray structure of BR up to 2.3 Å resolution (Pebay-Peyroula *et al*., 1997; Lücke *et al*., 1998; Essen *et al*., 1998). While the spatial arrangements of most of the residues in the protein core agree, significant differences exist in the loop regions. High temperature factors, especially of the residues in the E-F loop, prevented the resolution of the structure of this protein region in earlier work (Grigorieff *et al*., 1996; Pebay-Peyroula *et al*., 1997). A recent study revealed the structure of the E-F loop at 2.9 Å resolution (Essen *et al*., 1998), the experimental parameters, however, being far from physiological conditions. As experimental settings like temperature, pH and ionic strength as well as the lipid composition of the membrane may affect the conformation of the loops, it seems worthwhile to study their structure in their physiological environment and temperature using an alternative technique. Site-directed spin-labeling offers a complementary approach to identify elements of secondary and tertiary structure and follow structural changes with a time resolution in the millisecond range (Hubbell & Altenbach, 1994; Hubbell *et al*., 1996). In previous studies on bacteriorhodopsin, information on the secondary structure has been obtained by analysis of a consecutive series of spin-labeled cysteine mutants between residue positions 128 and 142 (Altenbach *et al*., 1990), and structural changes have been followed in all of the three cytoplasmic loops by introducing single spin-labeled cysteine residues and time-resolved EPR spectroscopy (Steinhoff *et al*., 1994; Rink *et al*., 1997). In the present approach, a systematic EPR study of the structure of the E-F loop is performed. A series of spin-labeled cysteine mutants in the region between residue positions 154 and 171 was prepared (Figure 1) and the structure characterized in terms of the spin label side-chain mobility and the accessibility for paramagnetic quenchers.

Results

Functional properties of the spin-labeled cysteine mutants

To monitor the integrity of the structure and function of the spin-labeled BR cysteine mutants, we analyzed the photocycle at 11 discrete wavelengths and focused on the second half of the photocycle. Differences in transient absorption changes during the photocycle are sensitive indicators for perturbations of functionally relevant structural domains. The recorded time-courses were analyzed using a global fitting procedure with a superposition of exponential functions (Rink *et al*., 1997). The apparent time-constants are num-

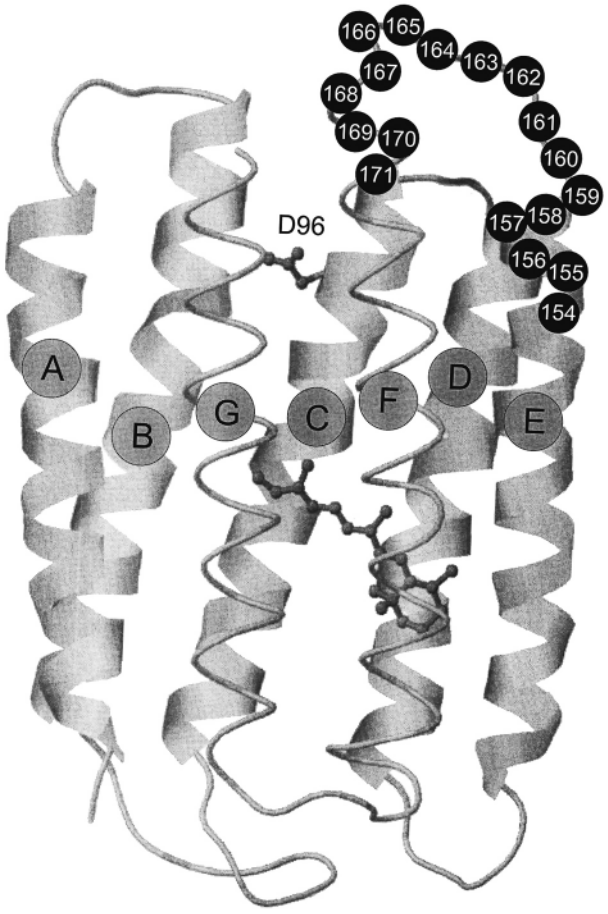

Figure 1. Model of the bacteriorhodopsin backbone according to Grigorieff *et al*. (1996). The amino acid residues that were exchanged by the spin-labeled cysteine mutants, the proton donor D96 and the retinal are indicated.

bered according to other authors (Hessling *et al*., 1993). For most of the mutants three relaxation times, τ_4, τ_3 and τ_6, were found to be sufficient to simulate the optical transients accompanying the M decay, which is the rate-limiting step of the cycle and thus determines the photocycle time. The values of these relaxation times and their contributions to the M decay are given in Table 1. The comparison of the decay times of the M intermediate for wild-type and spin-labeled samples shows that τ_3 and τ_4 varies less than 50 % for most of the mutants. Very fast M decays are found for R164R1, V167R1 and T170R1, which may be due to the steric influence of the nitroxide side-chain at the N terminus of helix F. The recovery of the BR initial state is largely delayed for the mutants T170R1 and F171R1. Here, a fourth time constant, τ_8, of the order of one second is necessary to fit the experimental data. The variation of the respective fractional contribution of each of the relaxations to the M decay reflects the fact that reversible equilibria exist between cycle intermediates (Varo & Lanyi, 1990), which may be influenced by mutations.

EPR spectra: mobility of the nitroxide side-chains

The shape of a spin-label EPR spectrum reflects the degree of reorientational motion of the nitroxide side-chain. This residual motion depends on the secondary and tertiary structure of the spin-label binding site and its vicinity. Weak interaction between the nitroxide and the rest of the protein results in a high degree of mobility. In this case, the apparent hyperfine splitting and the line width are small, as found for the spectra of E161R1, S162R1, R164R1 and E166R1 (Figure 2). In turn, if the residual motion is restricted due to strong interaction of the nitroxide group with neighboring side-chains or backbone atoms, the apparent hyperfine splitting and the line width are increased. This is obvious for the spectra of F154R1, G155R1, T157R1, A160R1, V167R1, S169R1, T170R1 and F171R1. The spectra of F156R1, S158R1, K159R1, M163R1, P165R1 and A168R1 clearly show two components corresponding to different nitroxide mobility. In general, the presented spectra cannot be simulated with a simple isotropic model of motion. Due to the interaction of the nitroxide with neighboring protein atoms the motion has to be assumed to be anisotropic, as was shown by molecular dynamics simulations (Steinhoff & Hubbell, 1996). Additionally, a distribution of motional states can be concluded from the spectra that exhibit more than one component. In spite of this complicated nature of the nitroxide dynamics, a simple mobility parameter, the inverse line width of the center line, has been found to be correlated with the structure of the binding-site environment (Hubbell & Altenbach, 1994; Hubbell *et al*., 1996). This parameter is shown in Figure 3(a) as a function of the sequence position. The highest motional restriction is visible in the region of the cytoplasmic parts of helices E (154-157) and F (167-171). In order to discriminate between intermolecular and intramolecular interaction, the spectra of two samples, T157R1 and S169R1, were additionally measured with the BR solubilized in octyl glucoside. BR has been found to be monomeric in this detergent (Dencher & Heyn, 1978). The inverse line width of the spectrum of T157R1 increased from 0.19 G^{-1} in the native membrane to 0.27 G^{-1} in the detergent, whereas that of S169R1 changed from 0.17 G^{-1} to

Table 1. Time constants and amplitudes of the M decay resulting from a multi-exponential fitting of the absorbance transients measured at 11 different wavelengths in the visible spectrum

Sample	τ_4 (ms)	τ_3 (ms)	τ_6 (ms)	$t_{1/2}$ (ms)
Wild-type	2.2 (33)	7.0 (67)	18 (0)	3.2
F154R1	2.2 (63)	9.0 (32)	63 (5)	2.4
G155R1	3.4 (17)	12 (72)	51 (11)	7.5
F156R1	3.0 (12)	12 (59)	63 (29)	10.3
T157R1	2.6 (58)	12 (38)	120 (4)	3.2
S158R1	2.4 (65)	12 (32)	100 (3)	2.7
K159R1	1.6 (87)	12 (13)	120 (0)	1.3
A160R1	2.3 (41)	11 (54)	82 (5)	3.9
E161R1	1.8 (56)	6.2 (42)	110 (2)	2.1
S162R1	1.8 (70)	7.8 (26)	32 (4)	1.8
M163R1	3.3 (61)	12 (38)	110 (1)	3.6
R164R1	1.1 (85)	6.7 (15)	31 (0)	0.9
P165R1	2.2 (54)	10 (40)	120 (6)	2.9
E166R1	1.8 (70)	12 (27)	83 (3)	1.9
V167R1	1.1 (85)	4.0 (15)	74 (0)	0.9
A168R1	3.4 (60)	12 (35)	130 (5)	3.8
S169R1	1.8 (80)	9.2 (18)	65 (2)	1.6
T170R1[a]	1.0 (84)	11 (19)	110 (2)	0.9
F171R1[a]	1.4 (75)	11 (24)	120 (4)	1.4

The respective relative amplitudes (percentage) found for a wavelength of 415 nm are given in parentheses. To facilitate comparison with published data, half times of the M decay are given in the last column.

[a] A fourth time constant, τ_8, is required to fit the recovery to the BR initial state: 1300 ms (−5 %) for T170R1 and 820 ins (−3 %) for F171R1.

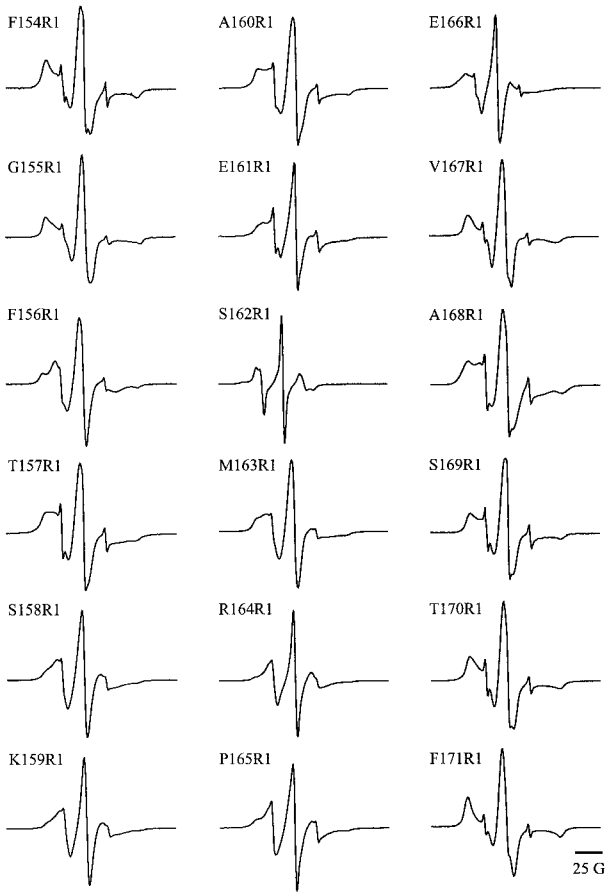

Figure 2. EPR spectra of spin-labeled BR mutants determined at room temperature.

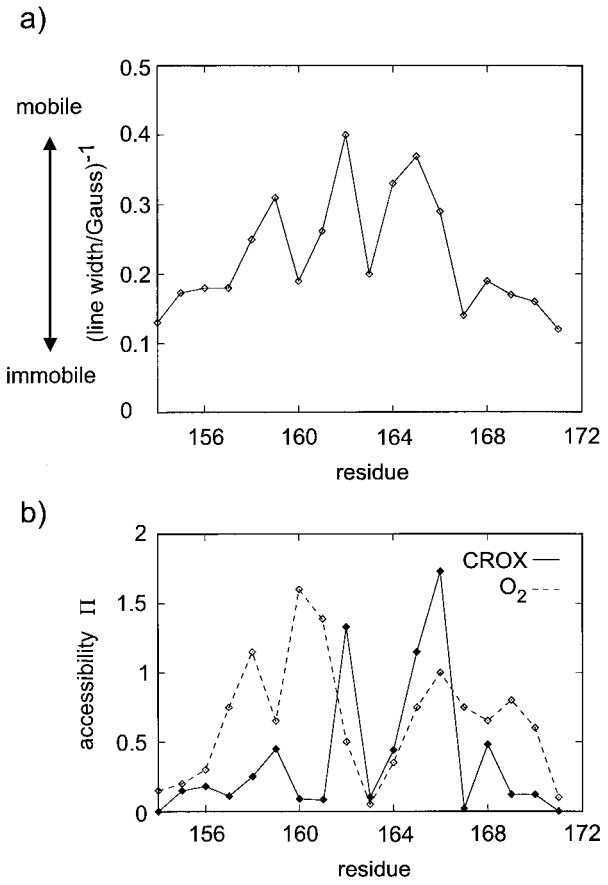

Figure 3. (a) The inverse line width of the center line of the spectra shown in Figure 2 plotted *versus* the position of the spin label in the BR sequence. The inverse line width is a measure of the spin label side-chain mobility. Small values represent immobile side-chains due to strong interactions of the nitroxide with neighboring protein atoms, high values represent a mobile spin label side-chain. (b) The accessibility parameter for chromium oxalate (continuous line, filled symbols) or oxygen (broken line, open symbols) *versus* sequence number. Π_{oxygen} was determined in equilibrium with air and scaled to pure oxygen; Π_{CROX} was measured in the presence of 50 mM CROX.

0.20 G^{-1}. This is strong evidence that the nitroxide at position 157 interacts with a neighboring BR molecule in the native membrane, whereas the interaction of the nitroxide at position 169 is mainly intramolecular. High nitroxide side-chain mobility is revealed for the loop positions 159, 161, 162, 164, 165 and 166. In contrast, the dynamics of the side-chain A160R1 and of one side-chain conformation of M163R1 is highly restricted, hence these nitroxide groups experience tertiary interactions with neighboring helices or loops.

Accessibilities to oxygen and chromium oxalate (CROX)

The motional analysis of elements of secondary and tertiary structure was supplemented by measuring the collision frequency of the nitroxide with a freely diffusing paramagnetic probe molecule. The collision frequency of such a probe depends on the product of its translational diffusion coefficient and its local concentration. Molecular oxygen and water-soluble chromium oxalate (CROX) have been frequently used and found to be ideally suited because of their sizes and solubility properties (Altenbach *et al.*, 1990; Farahbaksh *et al.*, 1992). Molecular oxygen has a low concentration in the tightly packed protein interior, whereas both the solubility and the diffusion coefficient are high in the bilayer. Therefore, the collision frequency between oxygen and spin labels in the interior of a protein is low, whereas it is high, if the spin label side-chain faces the bilayer. Likewise, it is possible to determine whether a spin label side-chain is located in the aqueous phase by measuring the collision frequency with the water-soluble CROX. The relative collision frequencies were determined by the method of continuous wave power saturation (Altenbach *et al.*, 1989). The accessibility parameter Π (see Materials and Methods) is proportional to the collision frequency of the nitroxide with the respective reagent.

The accessibility parameter values in the presence of CROX or with the sample in equilibrium

with air were plotted as a function of sequence position (Figure 3(b)). Classification was done according to the data given by Farahbakhsh *et al*. (1992) and Altenbach *et al*. (1990). The highest values of Π_{CROX} and hence the highest collision frequency with CROX is revealed for the side-chains attached to positions 159, 162, 164, 165, 166 and 168. Low values of Π_{CROX} were detected for residues at positions 154, 155, 156, 157, 158, 160, 161, 163, 167, 169, 170 and 171. The residues showing the largest collision frequency must be oriented towards the aqueous phase, while those with low values of Π_{CROX} face the protein or the bilayer. The accessibility parameter Π_{oxygen} and the width of the central absorption line allow discrimination between these cases. High values of the width of the center line and low oxygen accessibility is typical of the location of the nitroxide side-chain buried inside the protein. On the other hand, high motional freedom and thus narrow EPR lines combined with high oxygen accessibility are characteristic of the nitroxide in contact with the lipid bilayer. The oxygen accessibility is lowest for positions 154, 163 and 171. A comparably low value is also found for position 155. The nitroxide side-chains attached to these positions hence must be in the protein interior. The low accessibility for CROX in the region from 157 to 161, except 159, is accompanied by very high collision frequencies with oxygen. Hence, this is evidence for a location of the nitroxide with contact to the bilayer, where oxygen concentration is enhanced compared to the aqueous phase. To summarize the characteristics of the spin-labeled residues, Figure 4 shows a plot of the ratio of Π_{oxygen} to the line width *versus* Π_{CROX}. These two parameters define the coordinates of each side-chain on a two-dimensional surface that is divided into three areas, each one being typical of a side-chain exposed towards one of the three environments, water, lipid bilayer and protein interior. The division of Π_{oxygen} by the line width allows inclusion of the information on the nitroxide mobility in the two-dimensional plot. This facilitates the discrimination between nitroxide groups located in the protein interior, at the protein-lipid interface or sticking out into the lipid or aqueous phases. The phase boundary between lipid phase and aqueous phase has been arranged in order to maintain a constant Π_{CROX}/Π_{oxygen} ratio of about 0.7 (Farahbakhsh *et al*., 1992), which yields a nearly parabolic shape of the boundary. Due to different molecular sizes, a steric exclusion effect of CROX relative to the smaller oxygen molecule at the protein surface is most likely. Thus, the shown boundary between the protein and the aqueous phase has to be understood as the upper limit of the accessibility ratio. Residue T157C marks the boundary between the lipid bilayer and the protein, as its side-chain is oriented towards the intertrimer space with contact to a neighboring BR molecule (Grigorieff *et al*., 1996). Hence, the accessibility characteristics is determined by both protein and lipid contacts.

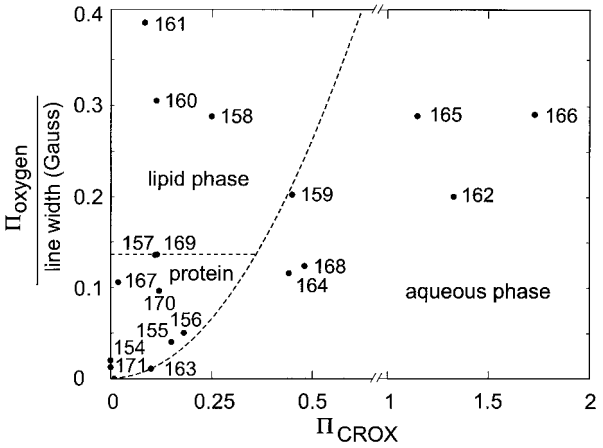

Figure 4. A two-dimensional plot of the ratio of Π_{oxygen} to the line width *versus* Π_{CROX} for each side-chain gives an overall view over the orientations of the side-chains in the E-F interhelical region. While the latter parameter is a direct measure for a side-chain orientation towards the water phase, the ratio of Π_{oxygen} to the line width discriminates between a lipid or protein environment for the spin-labeled residues. Hence, this plot contains three distinct areas typical of each protein, lipid or aqueous environment. For the position and the shape of the phase boundaries (broken lines), see the text.

Discussion

The knowledge of the spatial arrangement of the residues and their dynamics within a protein is essential for a full understanding of its function. X-ray crystallography and two-dimensional NMR spectroscopy have provided deep insight into the structure-function relationship of various proteins. However, the determination of the structures of membrane proteins is still a challenge, mainly due to the lack of a general approach for crystallization. Important exceptions are e.g. the photosynthetic reaction center and cytochrome *c* oxidase. An alternative method is cryo-electron microscopy, which has provided important structural data, especially on retinal proteins that were crystallized in two dimensions. Recently, X-ray data of BR were obtained from small crystals that were either grown in lipid cubic phases (Pebay-Peyroula *et al*., 1997; Lücke *et al*., 1998) or heterogeneously nucleated on the two-dimensional surface of an organic crystal (Essen *et al*., 1998). In addition to confirming the published structure proposals for the protein core (Grigorieff *et al*., 1996; Kimura *et al*., 1997) the work of Essen *et al*. (1998) yields new structural information about the cytoplasmic A-B, C-D and E-F loops. These data are of special interest, as time-resolved EPR experiments have revealed conformational changes of the loops during the M to N transition (Steinhoff *et al*., 1994; Mollaaghababa, 1995; Rink *et al*., 1997; Thorgeirsson *et al*., 1997). This structural change might be connected to the structural rearrangement of the helices observed by

time-resolved electron diffraction (Subramaniam *et al*., 1993; Han *et al*., 1994), X-ray diffraction (Koch *et al*., 1991), neutron diffraction experiments (Dencher *et al*., 1989) and FTIR spectroscopy (Souvignier & Gerwert, 1992; Ludlam *et al*., 1995). The question arises of whether the structure of the flexible loops as they are seen in the two or three-dimensional crystals are retained under more physiological conditions. Site-directed spin-labeling was used here to unravel the orientation of the side-chains of the E-F loop and its location with respect to the water lipid interface. We introduced single cysteine substitutions sequentially at positions 154 to 171. All mutants were then reacted with the cysteine-specific methanethiosulfonate spin label.

The orientation of the nitroxide side-chains is deduced from the classification according to their mobility and accessibility for paramagnetic quenchers as shown in Figure 4. The results for the nitroxide groups attached to the cytoplasmic ends of helices E and F (positions 155 to 157 and 166 to 171) are in nice agreement with published structural data sketched in Figure 5 (Grigorieff *et al*., 1996; Lücke *et al*., 1998; Essen *et al*., 1998). The side-chains attached to positions 155 and 156 face the protein interior, while those attached to 157 and 158 are oriented towards the lipid phase. Two spectral components are observed for F156R1 at the E-F helix-helix contact surface. These components may correspond to two conformations of the side-chain that are oriented towards the interior of the protein and towards the lipid bilayer, respectively. Strikingly, the motion of the nitroxide at position 157 is restricted. This side-chain interacts most probably with the G helix of a molecule in a neighboring trimer, since the spectrum of T157R1 solubilized in octyl glucoside exhibits an increased nitroxide dynamics. Position 159 is the first amino acid side-chain of the sequence that faces the aqueous phase. The high degree of mobility is strong evidence for its position in a loop region. A similar high degree of mobility is found for the nitroxide groups attached to positions 161, 162, 164, 165 and 166. According to the published X-ray data, the first residue in helical conformation belonging to helix F is 166. According to the EPR data, this amino acid residue is located in the aqueous phase. The reorientational motion of the nitroxide groups attached to 167 and 168 is strongly restricted by interaction with helices C and E, respectively. Similar to F156R1, the spectrum of A168R1 shows evidence for a second component of less motional restriction. This may correspond to a small fraction of molecules with the R1 side-chain oriented outward. Position 168 is still accessible for water-soluble quenchers. Positions 170 and 171 provide a location of the nitroxide already in the interior of the protein.

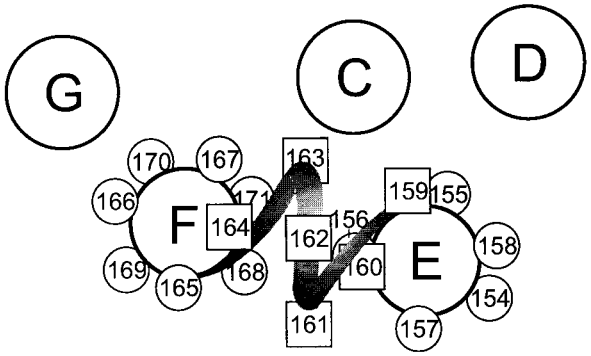

Figure 5. Projection of part of the cytoplasmic ends of the α-helices and the E-F loop of bacteriorhodopsin. Numbered symbols represent the C^{β} of residues that were studied by site-directed spin-labeling. The positions of the circles were taken from the structural data given by Grigorieff *et al*. (1996). Those residues symbolized by squares have been rearranged to be in agreement with the mobility and accessibility data determined by the EPR experiments.

High-resolution data of the E-F loop, which consists of residues 158 through 165, were not available from earlier studies (Grigorieff *et al*., 1996; Pebay-Peyroula *et al*., 1997). Due to high temperature factors, the structure of this region appeared to be disordered. These findings are in agreement with the EPR data, where the highest degree of mobility for certain nitroxide groups is found in the residue sequence from 158 to 165. Here, backbone flexibility and the residual motion of the side-chain contribute to the observed nitroxide mobility. However, spectral components corresponding to restricted motion are present, but to a different extent, and clearly dominate the spectra of A160R1 and M163R1. These components provide strong evidence for a side-chain conformation with the nitroxide side-chain oriented towards the protein. The arrangement of the loop residues 158 to 165 within a single turned and stretched loop as shown in Figure 5 is one possibility that agrees nicely with the experimental data. This arrangement is consistent with the structure model obtained recently from X-ray diffraction data by Essen *et al*. (1998).

We cannot exclude the possibility that the structure of the E-F loop is influenced by the exchange of native amino acids by the spin label side-chain R1. However, careful analysis of the photocycle of the modified protein shows that the functional properties reveal only minor changes. The comparison of the relaxation times and the corresponding relaxation amplitudes with those of the wild-type protein shows that the photocycle time of most of the mutants deviates from that of the wild-type by a factor of <2. The decreased M decay time τ_4 found for 167, 170 and 171, and the delayed back reaction to the BR initial state observed for 170 and 171 compared to the wild-type are most likely due to structural influences of the bulky spin label on the protein function. The side-chains of 167, 170 and 171 face the inter-helical region where a putative opening occurs during the M to N transition (Koch *et al*., 1991; Subramaniam *et al*., 1993). The steric interaction of the nitroxide with the protein may tilt helix F out. Consequently, a more

rapid reprotonation of the Schiff base occurs. The delay of the N-decay caused by the cysteine mutation and the spin label is pronounced for the mutants T170R1 and F171R1. This is in agreement with the results reported by Brown *et al*. (1995), who used maleimide labels to study the influence of bulky groups after attachment to helix F.

Thus, for solvent or lipid-exposed protein surface sites, substitution of the native side-chain by R1 produces little changes in the photocycle, except for charged residues that may be of functional importance. This is in agreement with findings reported by Mchaourab *et al*. (1996), that solvent-exposed sites and substitution of loop sites in phage T4 lysozyme by R1 were essentially without effect on the enzymatic activity and thermal stability. Even for most of the buried site mutants, the effect of R1 on the photocycle is small. The sequence-dependent variation of the EPR line shapes of the helical sites is consistent with the expectation based on previously determined BR structures. This indicates that the structural perturbation due to the introduction of R1 is small at the level of the backbone fold, even for the buried sites. Thus, we assume that the information obtained from the EPR spectra of R1 and from its accessibility for paramagnetic quenchers generally reflects the native BR structure at the level of the side-chain orientation.

The interpretation of the EPR line shape together with accessibility studies of the R1 side-chain provides a valuable tool for the solution of protein structures and dynamics. Despite the high temperature factors, which prevented resolution of the structure of the cytoplasmic E-F loop in earlier diffraction studies, EPR spectroscopy on a complete set of spin-labeled mutants yields a reasonable model for this protein region under physiological conditions. This model is in agreement with recent X-ray data reported by Essen *et al*. (1998), which can be considered as a confirmation of our methodical approach.

The presented initial state structure of the E-F loop domain is the starting point of the photocycle. The high sensitivity of the R1 side-chain mobility towards the changes in the relative positions of secondary elements involved in tertiary contact allow the detection of functionally related conformational changes with a time resolution in the millisecond range. Thus, a time-resolved EPR study of the whole set of spin-labeled mutants during the photocycle should reveal changes in the protein structure that eventually provide a basis for the complete understanding of the BR function.

Materials and Methods

Mutagenesis, expression and spin-labeling

Site-specific mutants of bacteriorhodopsin were prepared according to Ferrando *et al*. (1993). The codon of any chosen position, from 154 to 171, was changed to TGC, coding for cysteine, by means of site-directed mutagenesis by overlap extension. The PCR-product was cloned in the shuttle vector pUS-Mev (Schweiger, 1996). This vector is a derivative of the commercial vector pBluescript SK^- containing the *Hin*dIII-*Xho*I fragment from the vector pWL102 mediating resistance against mevinoline (Lam & Doolittle, 1989) and the *Bam* HI-*Hin*dIII fragment from pEF191 with the coding gene for bacterio-opsin (Ferrando *et al*., 1993). Homologous expression was followed by transformation of the *Halobacterium salinarum* strain SNOB, which is a bacterio-opsin gene-deficient derivative of the strain S9 (S9 without bop). Mutated proteins were isolated as purple membrane sheets according to Oesterhelt & Stoeckenius (1974). For confirmation of the *H. salinarum* transformants total DNA was isolated, and the bacterio-opsin gene amplified by PCR and sequenced.

The spin label (1-oxyl-2,2,5,5-tetramethylpyrroline-3-methyl)methanethiosulfonate (MTSSL; Reanal, Budapest) was covalently attached to the cysteine residues of the membrane-bound BR mutants to yield the spin label side-chain R1. For this purpose, 10 µl of a solution of 100 mM MTSSL in DMSO was added to 2.5 ml of suspension of membranes in 0.1 M phosphate buffer (pH 7.4), 0.1 M NaCl, resulting in a spin label to BR ratio of 10:1. The samples were then incubated at room temperature for 12 hours. Afterwards, the non-covalently bound spin label was removed by washing the membrane pellet several times with the buffer (25,000 *g* for 20 minutes). The labeled cysteine to BR ratio estimated from double integration of the EPR spectra and optical spectroscopy of BR was found to be close to 1 for all samples.

EPR and optical measurements

EPR spectra were recorded with a home-made X-band EPR spectrometer equipped with a Bruker dielectric resonator or a home-made loop gap resonator (Hubbell *et al*., 1987). A Bruker B-NM 12 B-field meter was used to adjust the magnetic field. The BR samples (5 µl) were loaded into EPR quartz capillaries at a final concentration of 200-500 µM. Spectra were taken at 293 K with a modulation amplitude of 1.5 G. After analog to 12 bit digital conversion, the data were processed in a personal computer. As a measure of the nitroxide mobility, the peak-peak line width of the center line was determined after subtraction of the sharp components resulting from a small amount of unbound spin label.

For power saturation experiments in the presence of oxygen or chromium oxalate (CROX), the samples were loaded into gas-permeable TPX capillaries (Jagmar Ltd., Krakṕw, Poland). The samples were deoxygenated by passing nitrogen around the sample capillary. For oxygen accessibility experiments, nitrogen was replaced by air. Saturation curves were determined from the peak-peak amplitudes of the center line measured at seven different incident microwave power levels in the range from 0.5 to 80 mW. The saturation behavior of the samples was parameterized by the quantity $P_{1/2}$, which is defined as the power level of the incident radiation at which the amplitude of the saturated line is half of the amplitude in absence of saturation. Values for this parameter were calculated by fitting the function:

$$A(P) = I\sqrt{P}(1 + (2^{1/\varepsilon} - 1)P/P_{1/2})^{-\varepsilon}$$

to the experimental amplitudes $A(P)$ according to the method of Altenbach *et al*. (1994). The scaling factor I and the measure of the saturation homogeneity ε are

adjustable parameters. The quantity $\Delta P_{1/2}$ is calculated from the difference in $P_{1/2}$ values in the presence and absence of the of relaxing agent. The $\Delta P_{1/2}$ values are divided by the peak-peak line width and normalized by the same quantity of a DPPH standard sample to obtain the dimensionless accessibility parameter Π.

Transient absorbance changes in the visible were recorded at 11 wavelengths between 405 nm and 665 nm (405, 415, 450, 470, 488, 515, 550, 580, 605, 635 and 665 nm) using a home-made optical set up. The concentration of the samples was adjusted to yield an A_{570} of about 0.8. Depending on the signal to noise ratio, the transient signals determined in the visible spectrum were sampled between 50 and 2000 times. The bandwidth of the amplifier was set to a time constant of 16 μs. The repetition rate was between 0.5 s^{-1} and 0.06 s^{-1} depending on the photocycle duration of the respective mutant. The time-course of the transient optical absorbance changes was analyzed by a global fitting procedure (Rink *et al.*, 1997).

Acknowledgments

We gratefully acknowledge the support of the Deutsche Forschungsgemeinschaft SFB 394, C1 and C2 (T.R., K.G. and H.-J. S.) and SFB 533, A4 (D. Oe.). H.J.S. greatly appreciates the support of Wayne L. Hubbell with the construction of the loop gap resonator.

References

Altenbach, C., Flitsch, S. L., Khorana, H. G. & Hubbell, W. L. (1989). Structural studies on transmembrane proteins. 2. Spin labeling of bacteriorhodopsin mutants at unique cysteines. *Biochemistry,* **28**, 7806-7812.

Altenbach, C., Marti, T., Khorana, H. G. & Hubbell, W. L. (1990). Transmembrane protein structure: spin labeling of bacteriorhodopsin mutants. *Science,* **248**, 1088-1092.

Altenbach, C., Greenhalgh, D. A., Khorana, H. G. & Hubbell, W. L. (1994). A collision gradient method to determine the immersion depth of nitroxides in lipid bilayers: application to spin-labeled mutants of bacteriorhodopsin. *Proc. Natl Acad. Sci. USA,* **91**, 1667-1671.

Brown, L. S., Varo, G., Needleman, R. & Lanyi, J. K. (1995). Functional significance of a protein conformation change at the cytoplasmic end of helix F during the bacteriorhodopsin photocycle. *Biophys. J.* **69**, 2103-2111.

Dencher, N. & Heyn, M. P. (1978). Formation and properties of bacteriorhodopsin monomers in the nonionic detergents octyl-beta-D-glucoside and Triton X-100. *FEBS Letters,* **96**, 322-326.

Dencher, N., Dresselhaus, G., Zaccai, G. & Büldt, G. (1989). Structural changes in bacteriorhodopsin during photon translocation revealed by neutron diffraction. *Proc. Natl Acad. Sci. USA,* **86**, 7876-7879.

Essen, L. O., Siegert, R., Lehmann, W. D. & Oesterhelt, D. (1998). Lipid patches in membrane protein oligomeres: crystal structure of the bacteriorhodopsin-lipid complex. *Proc. Natl Acad. Sci. USA,* **95**, 11673-11678.

Farahbakhsh, Z. T., Altenbach, C. & Hubbell, W. L. (1992). Spin labeled cysteines as sensors for protein-lipid interaction and conformation in rhodopsin. *Photochem. Photobiol.* **56**, 1019-1033.

Ferrando, E., Schweiger, U. J. & Oesterhelt, D. (1993). Homologous bacterio-opsin-encoding gene expression via site-specific vector integration. *Gene,* **125**, 41-47.

Grigorieff, N., Ceska, T. A., Downing, K. H., Baldwin, J. T. & Henderson, R. (1996). Electron-crystallographic refinement of the structure of bacteriorhodopsin. *J. Mol. Biol.* **259**, 393-421.

Han, B.-G., Vonck, J. & Glaeser, R. (1994). The bacteriorhodopsin photocycle: direct structural study of two substates of the M-intermediate. *Biophys. J.* **67**, 1179-1186.

Henderson, R., Baldwin, J. M., Ceska, T. A., Zemlin, F., Beckmann, E. & Downing, K. (1990). Model for the structure of bacteriorhodopsin based on high-resolution electron cryo-microscopy. *J. Mol. Biol.* **213**, 899-929.

Hessling, B., Souvignier, G. & Gerwert, K. (1993). A model-independent approach to assigning bacteriorhodopsin's intramolecular reactions to photocycle intermediates. *Biophys. J.* **65**, 1929-1941.

Hubbell, W. L. & Altenbach, C. (1994). Investigation of structure and dynamics in membrane proteins using site-directed spin labeling. *Curr. Opin. Struct. Biol.* **4**, 566-573.

Hubbell, W. L., Froncisz, W. & Hyde, J. S. (1987). Continuous and stopped flow EPR spectrometer based on a loop gap resonator. *Rev. Sci. Instrum.* **58**, 1879-1885.

Hubbell, W. L., Mchaourab, H. S., Altenbach, C. & Lietzow, M. A. (1996). Watching proteins move using site-directed spin labeling. *Structure,* **4**, 779-783.

Kimura, Y., Vassylyev, D. G., Miyazawa, A., Kidera, A., Matsushima, M., Mitsuoka, K., Murata, K., Hirai, T. & Fujiyoshi, Y. (1997). Surface of bacteriorhodopsin revealed by high-resolution electron crystallography. *Nature,* **389**, 206-211.

Koch, M. H. J., Dencher, N. A., Oesterhelt, D., Plön, H.-J., Rapp, G. & Büldt, G. (1991). Time-resolved X-ray diffraction study of structural changes associated with the photocycle of bacteriorhodopsin. *EMBO J.* **10**, 521-526.

Lam, W. L. & Doolittle, W. F. (1989). Shuttle vectors for the archaebacterium *Halobacterium volcanii*. *Proc. Natl Acad. Sci. USA,* **86**, 5478-5482.

Lanyi, J. K. (1993). Proton translocation mechanism and energetics in the light-driven pump bacteriorhodopsin. *Biochim. Biophys. Acta,* **1183**, 241-261.

Lozier, R. H., Xie, A., Hofrichter, J. & Clore, G. M. (1992). Reversible steps in the bacteriorhodopsin photocycle. *Proc. Natl Acad. Sci. USA,* **89**, 610-614.

Ludlam, C. F., Sonar, S., Lee, C. P., Coleman, M., Herzfeld, J., RajBhandary, U. L. & Rothschild, K. J. (1995). Site-directed isotope labeling and ATR-FTIR difference spectroscopy of bacteriorhodopsin: the peptide carbonyl group of Tyr185 is structurally active during the bR → N transition. *Biochemistry,* **34**, 2-6.

Lücke, H., Richter, H.-T. & Lanyi, J. K. (1998). Proton transfer pathways in bacteriorhodopsin at 2.3 angstrom resolution. *Science,* **280**, 1934-1937.

Mchaourab, H. S., Lietzow, M. A., Hideg, K. & Hubbell, W. L. (1996). Motion of spin-labeled side chains in T4 lysozyme. Correlation with protein structure and dynamics. *Biochemistry,* **35**, 7692-7704.

Mollaaghababa, R. (1995). Functional and time-resolved structural studies of bacteriorhodopsin mutants following expression in *Halobacterium halobium*. PhD thesis, Massachusetts Institute of Technology, Cambridge, USA.

Oesterhelt, D. (1998). Structure and mechanism of the family of retinal proteins from halophilic archaea. *Curr. Opin. Struct. Biol.* **8**, 489-500.

Oesterhelt, D. & Stoeckenius, W. (1974). Isolation of the cell membrane of *Halobacterium halobium* and its fraction into red and purple membrane. *Methods Enzymol.* **31**, 667-686.

Pebay-Peyroula, E., Rummel, G., Rosenbusch, J. P. & Landau, E. M. (1997). X-ray structure of bacteriorhodopsin at 2.5 angstroms from microcrystals grown in lipidic cubic phases. *Science,* **277**, 1676-1681.

Rink, T., Riesle, J., Oesterhelt, D., Gerwert, K. & Steinhoff, H.-J. (1997). Spin labeling studies of the conformational changes in the vicinity of D36, D38, T46 and E161 of bacteriorhodopsin during the photocycle. *Biophys. J.* **73**, 983-993.

Sass, H. J., Schachowa, I., Rapp, G., Koch, M., Oesterhelt, D., Büldt, G. & Dencher, N. A. (1997). The tertiary structural changes in bacteriorhodopsin occur between M states: X-ray diffraction and fourier-transform infrared spectroscopy. *EMBO J.* **16**, 1484-1491.

Schweiger, U. (1996). Funktionelle Charakterisierung der Retinalbindungstasche von Bakteriorhodopsin durch spezifische Mutangenese. PhD thesis, Leopold-Franzens-Universität, Innsbruck, Austria.

Souvignier, G. & Gerwert, K. (1992). Proton uptake mechanism of bacteriorhodopsin as determined by time-resolved stroboscopic-FTIR-spectroscopy. *Biophys. J.* **63**, 1393-1405.

Steinhoff, H.-J. & Hubbell, W. L. (1996). Calculation of electron paramagnetic resonance spectra from Brownian dynamics trajectories: application to nitroxide side chains in proteins. *Biophys. J.* **71**, 2201-2212.

Steinhoff, H.-J., Mollaaghababa, R., Altenbach, C., Hideg, K., Krebs, M., Khorana, H. G. & Hubbell, W. L. (1994). Time-resolved detection of structural changes during the photocycle of spin-labeled bacteriorhodopsin. *Science,* **266**, 105-107.

Subramanian, S., Gerstein, M., Oesterhelt, D. & Henderson, R. (1993). Electron diffraction analysis of structural changes in the photocycle of bacteriorhodopsin. *EMBO J.* **12**, 1-8.

Thorgeirsson, T. E., Xiao, W., Brown, L. S., Needleman, R., Lanyi, J. K. & Shin, Y.-K. (1997). Transient channel-opening in bacteriorhodopsin: an EPR study. *J. Mol. Biol.* **273**, 951-957.

Tittor, J. (1991). A new view of an old pump: bacteriorhodopsin. *Curr. Biol.* **1**, 534-538.

Varo, G. & Lanyi, J. K. (1990). Pathways of the rise and decay of the M photointermediate(s) of bacteriorhodopsin. *Biochemistry,* **30**, 5016-5022.

Varo, G. & Lanyi, J. K. (1991). Kinetic and spectroscopic evidence for an irreversible step between reprotonation and deprotonation of the schiff base in the bacteriorhodopsin photocycle. *Biochemistry,* **30**, 5008-5015.

Wikström, M. (1998). Proton translocation by bacteriorhodopsin and heme-copper oxidases. *Curr. Opin. Struct. Biol.* **8**, 480-488.

Xie, A. H., Nagle, J. F. & Lozier, R. H. (1987). Flash spectroscopy of purple membrane. *Biophys. J.* **51**, 627-635.

Edited by W. Baumeister

(Received 24 August 1998; received in revised form 25 January 1999; accepted 25 January 1999)